**Atmospheric
Chemistry
and Physics
Discussions**

A case study of dust aerosol radiative properties over Lanzhou, China

L. Zhang, X. Cao, J. Bao, B. Zhou, J. Huang, J. Shi, and J. Bi

Key Laboratory for Semi-Arid Climate Change of the Ministry of Education, College of
Atmospheric Sciences, Lanzhou University, Lanzhou, 730000, China

Correspondence to: L. Zhang (zhanglei@lzu.edu.cn)

ACPD

10, 2889–2914, 2010

**A case study of dust
aerosol radiative
properties over
Lanzhou, China**

L. Zhang et al.

Title Page

Abstract	Introduction
Conclusions	References
Tables	Figures

| ◄◄ | ►► |
| ◄ | ► |

Back | Close

Full Screen / Esc

Printer-friendly Version

Interactive Discussion

A case study of dust aerosol radiative properties over Lanzhou, China

L. Zhang et al.

Abstract

The vertical distribution of dust aerosol and its radiative properties are analysed using the data measured by the micropulse lidar, profiling microwave radiometer, sunphotometer, particulate monitor, and nephelometer at the Semi-Arid Climate and Environment Observatory of Lanzhou University (SACOL) during a dust storm from 27 March to 29 March 2007. The analysis shows that the dust aerosol mainly exists below 2 km in height, and the dust aerosol extinction coefficient decreases with height. The temporal evolution of aerosol optical depth (AOD) during the dust storm is characterized by a sub-maximum at 22:00 (Beijing Time) on 27 March and a maximum at 12:00 on 28 March. The AOD derived by lidar is compared with that obtained by sunphotometer, and shows a good consistency. The PM_{10} concentration and aerosol scattering coefficient share identical variation trends, and their maximums both appear at 22:00 on 27 March.

The aerosol extinction coefficient and relative humidity have the same trends and their maximums appear at identical heights, showing a correlation between extinction coefficient and relative humidity known as aerosol hygroscopicity. Nevertheless, the correlation between aerosol extinction coefficient and temperature cannot be obviously seen.

The aerosol extinction coefficient, scattering coefficient, and PM_{10} concentration present good linear correlations. The correlation coefficients of the aerosol scattering coefficient and PM_{10} concentration, of aerosol extinction coefficient and PM_{10} concentration, and of aerosol extinction and scattering coefficient are respectively 0.98, 0.94, and 0.96.

1 Introduction

Natural and anthropogenic aerosol plays a crucial role in the global and regional climate (Pappalardo et al., 2003). Aerosol affects the Earth and atmospheric radiation

budget by directly scattering and absorbing the incoming solar radiation (McCormick and Ludwig, 1967; Charlson and Pilat, 1969; Atwater, 1970; Coakley et al., 1983) and by indirectly increasing the cloud albedo and suppressing precipitation by modifying cloud microphysical properties as cloud condensation nuclei (Twomey, 1977; Albrecht, 1989). The direct aerosol effect will influence the atmospheric temperature structure and cloud formation (Grassl, 1975; Hansen et al., 1997; Ackerman et al., 2000; Koren et al., 2004).

Dust storms occur frequently in spring and winter in the severe desertification regions. Dust aerosol is a chief contributor to the global aerosol loading (Pierangelo et al., 2004). The dust aerosol severely affects the local climate and environment by influencing the atmospheric radiation balance and decreasing atmospheric visibility (Wang et al., 2005). Recent years have witnessed numerous studies on the aerosol radiative properties (Blanco et al., 2003; Gobbi et al., 2003; Immler et al., 2003; Collaud Coen et al., 2004; Papayannis et al., 2005; Balkanski et al., 2007; Zhang et al., 2007; Su et al., 2008; Hong et al., 2008).

Some aerosol field experiments have also been carried out over the arid region of China, and much research progress has been made (e.g. Iwasaka et al., 2003; Yamada et al., 2005; Shen et al., 2006; Huang et al., 2009; Liu et al., 2002a). However few observations were carried out over the semiarid region of the Loess Plateau. In order to improve the understanding of the impact of human activity on semiarid climate, the Semi-Arid Climate and Environment Observatory of Lanzhou University (SACOL, 35°57′ N, 104°08′ E, 1965.8 m) was established in 2005 (Huang et al., 2008a). SACOL measures wind-blown dust and air pollution aerosol radiative properties, especially the dust aerosol effect.

The paper aims to analyse the dust aerosol radiative properties using the data collected by the micropulse lidar, profiling microwave radiometer, sunphotometer, particulate monitor, and nephelometer at SACOL during a dust storm from 27 March to 29 March 2007.

2 Instrumentation

The micropulse lidar (CE370-2) is a full-time and long-term unattended automatically operated system which is a co-axial system with a 20 cm diameter telescope and employs a Q-switched frequency doubled Nd: YAG laser operated at 532 nm. The pulse repetition frequency is configured at 4.7 kHz. The detector is operated in photon-counting mode with a quantum efficiency approaching 55% and maximum count rate near to 20 MHz. The micropulse lidar is capable of obtaining the aerosol vertical profiles from ground up to 30 km (maximum) height with a range resolution of 15 m.

The profiling microwave radiometer (TP/WVP-3000) is a passive remote sensing instrument. It has two profiling systems for temperature and relative humidity, and uses the atmospheric radiation in the frequency band of 22–60 GHz, of which 22–30 GHz is for water vapour profile and 51–59 GHz for temperature profile. It can obtain the vertical profiles of temperature, water vapour, and liquid water from ground to 10 km height with a time resolution of 1 min and range resolutions of 0.1 km for the height below 1 km and 0.25 km for 1–10 km.

The sunphotometer (CE-318) measures the direct and scattering solar irradiance in the visible and near infrared wavelengths, respectively 1020, 870p1, 670, 440, 870p2, 870, 936, and 870p3 nm, of which the bandwidth is 10 nm. It determines the atmospheric spectral transmission, scattering properties, and precipitable water. Its optical head has a sun collimator and sky collimator with a field-of-view of 1.2°. The sun tracking is realised by the evaluation of the solar altitude with a four-quadrant detector. It is now widely used in atmospheric sciences to determine aerosol properties like AOD, Ångström exponent, and precipitable water, which can be applied to the validation of satellite remote sensing.

The particulate monitor (TEOM 1400a) measures PM_{10} concentration in real-time and in the long term. It uses a static balance to monitor the frequency change, which can be inversed to mass concentration. The nephelometer (M9003) observes the aerosol light scattering coefficient at three wavelengths of 450, 520, and 700 nm. The

A case study of dust aerosol radiative properties over Lanzhou, China

L. Zhang et al.

relative humidity of sample air is controlled below 60% to eliminate its impact on scattering. Background and span calibrations are performed periodically to ensure the data quality.

3 Lidar retrieval method

An inversion algorithm is modified on the basis of the retrieval method of Klett (1981, 1985) and Fernald (1984) to distinguish the aerosol extinction coefficient from that of the atmospheric molecules. The lidar equation for aerosol scattering and molecular scattering is:

$$P(z) = E \cdot C \cdot z^{-2} [\beta_1(z) + \beta_2(z)] \cdot T_1^2(z) \cdot T_2^2(z) \tag{1}$$

where z is the range, $P(z)$ the lidar return signal scattered by aerosol and atmospheric molecules, E the output laser pulse energy, C the calibration constant, $\beta(z)$ the backscattering coefficient, $T(z) = \exp\left[-\int_0^z \sigma(z) dz\right]$ the transmittance, and $\sigma(z)$ the extinction coefficient. There the subscript 1 stands for the aerosol while 2 stands for the atmospheric molecules. σ_2 can be obtained using the Rayleigh scattering theory. Then the solution of Eq. (1) for the aerosol backscattering is as follows:

$$\beta_1(z) = \frac{P(z)z^2 \exp\left[-2(S_1-S_2)\int_0^z \beta_2(z) dz\right]}{CE - 2S_1 \int_0^z P(z)z^2 \exp\left[-2(S_1-S_2)\int_0^z \beta_2(z') dz'\right] dz} - \beta_2(z) \tag{2}$$

If prior information on the aerosol extinction coefficient is available at the reference height z_c, then the aerosol extinction coefficient at z which is below z_c can be obtained from Eq. (3) (backward solution):

$$\sigma_1(z) = -\frac{S_1}{S_2} \cdot \sigma_2(z) + \frac{X(z) \cdot \exp\left[2\left(\frac{S_1}{S_2}-1\right)\int_z^{z_c} \sigma_2(z') dz'\right]}{\frac{X(z_c)}{\sigma_1(z_c) + \frac{S_1}{S_2}\sigma_2(z_c)} + 2\int_z^{z_c} X(z')\exp\left[2\left(\frac{S_1}{S_2}-1\right)\int_z^{z_c} \sigma_2(z'') dz''\right] dz'} \tag{3}$$

As to the aerosol extinction coefficient at z which is above z_c, it can be derived from Eq. (4) (forward solution):

$$\sigma_1(z) = -\frac{S_1}{S_2} \cdot \sigma_2(z) + \frac{X(z) \cdot \exp\left[-2\left(\frac{S_1}{S_2}-1\right)\int_{z_c}^{z}\sigma_2(z')dz'\right]}{\frac{X(z_c)}{\sigma_1(z_c) + \frac{S_1}{S_2}\sigma_2(z_c)} - 2\int_{z_c}^{z}X(z')\exp\left[-2\left(\frac{S_1}{S_2}-1\right)\int_{z_c}^{z}\sigma_2(z'')dz''\right]dz'} \quad (4)$$

where $X(z)=P(z)z^2$ indicates the range normalized lidar return signal, and S_1 the aerosol extinction-to-backscatter ratio, or lidar ratio (LR), while S_2, the corresponding extinction-to-backscatter ratio for the atmospheric molecules, is set at 8 $\pi/3$.

In the retrieval, an LR must be a priori assumed, which makes the retrieved aerosol extinction and backscattering coefficient more relative than absolute (Larchevêque et al., 2002). Generally LR is determined by the aerosol size distribution, shape, and composition (He et al., 2006). LR varies temporally and spatially due to the inhomogeneous distribution of aerosol and cloud (Ansmann et al., 1992). Kovalev (1995) shows that an incorrectly assumed LR will significantly corrupt the retrieval under the inhomogeneous aerosol conditions.

A number of researches have been conducted in recent years with Raman lidar or high spectral resolution lidar to measure LR in different sites. LR generally ranges from 20 to 100 sr (Balis et al., 2004). LR is 47±15 sr (532 nm) for the background aerosol and 44±19 sr for dust aerosol in Korea (Chiang et al., 2008), while Liu et al. (2002b) derive LR of Asian dust aerosol to be 42–55 sr (532 nm). As for the Saharan dust aerosol, its LR is 45 sr (532 nm) (Immler and Schrems, 2003). Using a micropulse lidar and MODIS data, He et al. (2006) retrieve the LR of Hong Kong to be 18–44 sr (523 nm), with a mean of 29.1±5.8 sr. Also Ackermann (1998) makes a numerical study of LR, and presents LRs of 40–80 sr for continental aerosol, 15–30 sr for maritime aerosol, and 17–25 sr for dust aerosol (532 nm). There are also some previous studies about the LR in Lanzhou (Xia, 2006; Han, 2007), and hence a value of 25 sr for LR is selected in the retrieval.

The determination of the reference height is another important assumption, and can be taken in the region where the lidar return signal is followed by molecular atmosphere. Klett (1981) shows that the backward solution is generally stable. Therefore, in this retrieval, the backward solution is selected.

4 Results

The dust storm arrived in Lanzhou at 20:00 (Beijing Time, 1 h and 3 min earlier than Lanzhou local time) on 27 March and ended at 16:00 on 29 March 2007. Figure 1 shows the wind direction and speed from 00:00 on 27 March to 23:30 on 29 March, which were observed by a three-axis sonic anemometer set up at SACOL 3 m above the ground every 30 min. Southeast wind was dominant over SACOL and the speed ranged from 1.0 to 3.0 m/s. The relative humidity and temperature shown in Fig. 2 were measured by the profiling microwave radiometer. The relative humidity during the dust storm was obviously smaller than that before the dust storm, which indicates an impact of dust aerosol on the local atmospheric condition.

4.1 Vertical structure of dust aerosol

Figure 3 presents the temporal evolution of the lidar backscattering signal vertical section from 08:00 (Beijing Time) on 27 March to 20:00 on 29 March. It can clearly distinguish the aerosol layer from clouds. Before 20:00 on 27 March, the aerosol loading was not heavy, and clouds over 5 km could be observed by lidar. When the dust storm occurred, the lidar detecting height would be reduced; the aerosol was thus mainly concentrated in the low layer, and the lidar backscattering signal became bigger. In this case the dust aerosol was mainly distributed in the layer under 2 km, where the aerosol concentration was relatively high.

Figure 4 presents four different cases for the vertical profiles of dust aerosol extinction coefficient. Firstly the dust aerosol extinction coefficient decreased rapidly with

height. The lidar detecting range decreased severely due to the high dust aerosol concentration. From the vertical profiles it can be observed that the dust aerosol was concentrated in the layer below 2 km height, which shows consistency with the results of Fig. 3. Regarding the dust aerosol extinction coefficient value, the maximum was 3.16 km^{-1} at 0.195 km height. When the dust storm declined at 12:13 on 29 March, it decreased to 0.62 km^{-1} at 0.195 km.

The paper here discusses the dust aerosol layer below 2 km height. In comparison with the ground-based network observations made by Murayama et al. (2001) of Asian dust and the vertical distribution analysis of the dust storm in April 1998, the dust height was about 3 km over Japan, 4 to 5 km in Seoul and Hefei, and even in the upper troposphere over Japan and Hefei. Thus it is shown that the higher the aerosol height, the further the dust can be sent.

4.2 AOD temporal evolution

Figure 5 shows the temporal evolution of AOD retrieved by micropulse lidar from 08:00 (Beijing Time) on 27 March to 16:00 on 29 March. Since the duration between 08:00 and 20:00 on 27 March had no dust storm, AOD ranged from 0.3 to 0.4. The result presents the background aerosol properties over Lanzhou and has a good agreement with the result of Huang et al. (2008b). When the dust storm occurred at 20:00 on 27 March, the AOD increased with rapidity to 0.63, which was obviously due to the impact of dust aerosol. Then it reached a sub-maximum of 0.94 at 22:00 on 27 March, decreased afterwards to the minimum of 0.72 at 02:20 on 28 March, and then increased rapidly again to the maximum of 1.95 at 12:00 on 28 March. Then it gradually diminished until the end of the dust storm. Comparison of Figs. 3 and 5 shows a good consistency.

A case study of dust aerosol radiative properties over Lanzhou, China

L. Zhang et al.

4.3 Comparison of AOD derived by lidar and sunphotometer

From the Beer-Lambert-Bouguer law, the total optical depth can be retrieved using the solar direct radiation measured by sunphotometer. It is composed of aerosol, atmospheric absorption, and scattering optical depth. The atmospheric scattering optical depth can be calculated using Rayleigh scattering theory, whereas the atmospheric absorption optical depth is rather complicated. Therefore, the wavelengths at which the atmospheric absorption can be ignored are determined. Then the AOD of these wavelengths can be calculated by subtracting the atmospheric scattering optical depth from the total optical depth. For the comparison between the AOD derived by micropulse lidar and sunphotometer, the AOD of the sunphotometer at 532 nm can be obtained by interpolation using Eq. (5) and the AOD at other three wavelengths such as 440, 675, and 870 nm from AERONET.

$$\ln[\mathrm{AOD}(\lambda)] = a_1 + a_2 \ln(\lambda) + a_3 [\ln(\lambda)]^2 \tag{5}$$

Figure 6 presents a comparison between the AOD derived by micropulse lidar and sunphotometer using the simultaneously collected data of the period before the dust storm and near the end of the dust storm, because the sunphotometer measurement was severely affected by the dust aerosol. It can be easily seen that the difference between the two retrievals is slight and there exists a good consistency.

In order to further a quantitative comparison between lidar and sunphotometer retrievals, the absolute difference, relative difference, ratio difference, and their mean are calculated. The details are illustrated in Table 1. The absolute difference is rather small in general, with only two exceptions over 0.13, which were at 08:50 (Beijing Time) and 10:17 on 29 March. The mean absolute difference is 0.041. The mean relative difference is 12.0%. The mean ratio difference is −0.055, which means that the AOD derived by lidar is slightly bigger than that by sunphotometer.

4.4   Temporal evolution of PM$_{10}$ concentration and scattering coefficient

Figure 7 gives a temporal evolution of PM$_{10}$ concentration and aerosol scattering coefficient every 5 min from 08:00 (Beijing Time) on 27 March to 18:30 on 29 March. Before 20:00 on 27 March when there was no dust, the PM$_{10}$ concentration was mainly below
0.3 mg/m^3. Then it increased sharply to the maximum at 22:00 with a PM$_{10}$ concentration of 8.836 mg/m^3. Afterwards the PM$_{10}$ concentration decreased. The background aerosol scattering coefficient was mainly below 0.2 km^{-1}. The maximum aerosol scattering coefficients of 450, 520, and 700 nm were 3.045, 2.441, and 1.233 km^{-1} respectively at 22:00 on 27 March, which were same as those when the PM$_{10}$ concentration reached the maximum. Then it decreased until the end of the dust storm with a sub-maximum at 12:00 on 28 March, when the scattering coefficients of 450, 550, and 700 nm were 1.383, 1.162, and 0.537 km^{-1} respectively. Comparing Fig. 7 with Fig. 5, the maximums of AOD, PM$_{10}$ concentration, and aerosol scattering coefficient appeared at exactly the same time. The temporal evolutions of the aerosol scattering coefficient at three different wavelengths show a good agreement. The comparison of the aerosol scattering coefficient and PM$_{10}$ concentration also shows an identical variation.

4.5   Relationship between aerosol extinction coefficient, relative humidity, and temperature

Figure 8 presents the profiles of the dust aerosol extinction coefficient (DAEC), relative humidity (RH), and temperature (T) for four different cases. The relative humidity increased slowly with height to the maximum at 0.3 km, then decreased quickly to the minimum at about 1.0 km, and then increased again. The temperature vertical profiles showed a decreasing trend.

As analysed above, the dust aerosol mainly existed in the layer below 2 km, in which the relative humidity profile had an identical variation trend with the dust aerosol extinction coefficient, and the maximums of the dust aerosol extinction coefficient and relative

A case study of dust aerosol radiative properties over Lanzhou, China

L. Zhang et al.

humidity appeared at exactly the same height. This shows a correlation between relative humidity and the aerosol extinction coefficient known as aerosol hygroscopicity, which demonstrates higher relative humidity higher extinction. However the correlation between the dust aerosol extinction coefficient and temperature is not obviously seen.

4.6 Correlation analysis among PM_{10} concentration, aerosol extinction, and scattering coefficient

Figure 9 shows the correlation among PM_{10} concentration, aerosol extinction coefficient, and scattering coefficient. Obviously PM_{10} concentration and aerosol scattering coefficients of 450, 520, and 700 nm have a very good linear correlation as shown in Fig. 9a, and the correlation coefficient is 0.98.

The aerosol extinction coefficient reflects the total effect of aerosol absorption and scattering. Taking these two elements into consideration, a comprehensive understanding can be made of how the aerosol affects the atmospheric radiation balance and climate change. Figure 9b and c show the correlation between aerosol extinction coefficient and PM_{10} concentration, and correlation between aerosol extinction and scattering coefficient. They have good linear correlations, and the correlation coefficient between aerosol extinction coefficient and PM_{10} concentration is 0.94, while that for the correlation between aerosol extinction coefficient and scattering coefficient is 0.96.

5 Summary and discussion

The dust aerosol radiative properties over Lanzhou are analysed through a case study of the dust storm from 27 March to 29 March 2007 using the data collected by micropulse lidar, profiling microwave radiometer, sunphotometer, particulate monitor, and nephelometer at SACOL.

The dust aerosol is mainly concentrated in the region under 2 km in height. The dust aerosol extinction coefficient decreases with height. As for the temporal evolution of AOD, its sub-maximum appears at 22:00 (Beijing Time) on 27 March and its maximum at 12:00 on 28 March. The comparison between AOD derived by micropulse lidar and sunphotometer shows a good consistency. The aerosol scattering coefficient and PM_{10} concentration present identical trends, with the maximums appearing at 22:00 on 27 March.

The aerosol extinction coefficient and relative humidity have the same trends and their maximums appear at exactly the same height, which shows the correlation between aerosol extinction coefficient and relative humidity known as aerosol hygroscopicity. However the correlation between aerosol extinction coefficient and temperature is not obvious.

The aerosol extinction coefficient, scattering coefficient, and PM_{10} concentration present good linear correlations. The correlation coefficient between the aerosol scattering coefficient and PM_{10} concentration is 0.98, while that for the correlation between aerosol extinction coefficient and PM_{10} concentration is 0.94, and that for the correlation between aerosol extinction coefficient and scattering coefficient is 0.96.

Nevertheless, due to the data limitation, the paper only presents a dust aerosol case study. Further and more comprehensive observations are still needed in the application of lidar and other instruments to explore the dust aerosol radiative forcing.

References

Ackerman, A. S., Toon, O. B., Stevens, D. E., Heymsfield, A. J., Ramanathan, V., and Welton, E. J.: Reduction of tropical cloudiness by soot, Science, 288(5468), 1042–1047, 2000.

Ackermann, J.: The extinction-to-backscatter ratio of tropospheric aerosols: a numerical study, J. Atmos. Ocean. Tech., 15, 1043–1050, 1998.

Albrecht, B. A.: Aerosols, cloud microphysics, and fractional cloudiness, Science, 245(4923), 1227–1230, 1989.

Ansmann, A., Riebesell, M., Wandinger, U., Weitkamp, C., Voss, E., Lahmann, W., and Michaelis, W.: Combined Raman elastic-backscatter lidar for vertical profiling of moisture, aerosol extinction, backscatter, and lidar ratio, Appl. Phys. B, 55, 18–28, 1992.

Atwater, M. A.: Planetary albedo changes due to aerosols, Science, 170(3953), 64–66, 1970.

Balis, D. S., Amiridis, V., Nickovic, S., Papayannis, A., and Zerefos, C.: Optical properties of Saharan dust layers as detected by a Raman lidar at Thessaloniki, Greece, Geophys. Res. Lett., 31, L13104, doi:10.1029/2004GL019881, 2004.

Balkanski, Y., Schulz, M., Claquin, T., and Guibert, S.: Reevaluation of Mineral aerosol radiative forcings suggests a better agreement with satellite and AERONET data, Atmos. Chem. Phys., 7, 81–95, 2007,
http://www.atmos-chem-phys.net/7/81/2007/.

Blanco, A., Dee Tomasi, F., Filippo, E., Manno, D., Perrone, M. R., Serra, A., Tafuro, A. M., and Tepore, A.: Characterization of African dust over southern Italy, Atmos. Chem. Phys., 3, 2147–2159, 2003,
http://www.atmos-chem-phys.net/3/2147/2003/.

Charlson, R. J. and Pilat, M. J.: Climate: The influence of aerosols, J. Appl. Meteorol., 8(6), 1001–1002, 1969.

Chiang, C. W., Das, S. K., and Nee, J. B.: An iterative calculation to derive extinction-to-backscatter ratio based on lidar measurements, J. Quant. Spectrosc. Ra., 109, 1187–1195, 2008.

Coakley Jr., J. A., Cess, R. D., and Yurevich, F. B.: The effect of tropospheric aerosols on the earth's radiation budget: a parameterization for climate models, J. Atmos. Sci., 40(1), 116–138, 1983.

Collaud Coen, M., Weingartner, E., Schaub, D., Hueglin, C., Corrigan, C., Henning, S., Schwikowski, M., and Baltensperger, U.: Saharan dust events at the Jungfraujoch: detection

by wavelength dependence of the single scattering albedo and first climatology analysis, Atmos. Chem. Phys., 4, 2465–2480, 2004, http://www.atmos-chem-phys.net/4/2465/2004/.

Fernald, F. G.: Analysis of atmospheric lidar observations: some comments, Appl. Optics, 23(5), 652–653, 1984.

Gobbi, G. P., Barnaba, F., Van Dingenen, R., Putaud, J. P., Mircea, M., and Facchini, M. C.: Lidar and in situ observations of continental and Saharan aerosol: closure analysis of particles optical and physical properties, Atmos. Chem. Phys., 3, 2161–2172, 2003, http://www.atmos-chem-phys.net/3/2161/2003/.

Grassl, H.: Albedo reduction and radiative heating of clouds by absorbing aerosol particles, Contrib. Atmos. Phys., 48, 199–210, 1975.

Han, X.: Retrieval of Lanzhou urban and suburban aerosol radiative properties using lidar measurement, M. S. thesis, Lanzhou University, China, 51 pp., 2007.

Hansen, J., Sato, M., and Ruedy, R.: Radiative forcing and climate response, J. Geophys. Res., 102(D6), 6831–6864, 1997.

He, Q. S., Li, C. C., Mao, J. T., Lau, A. K. H., and Li, P. R.: A study on the aerosol extinction-to-backscatter ratio with combination of micro-pulse LIDAR and MODIS over Hong Kong, Atmos. Chem. Phys., 6, 3243–3256, 2006, http://www.atmos-chem-phys.net/6/3243/2006/.

Hong, G., Yang, P., Weng, F. Z., and Liu, Q. H.: Microwave scattering properties of sand particles: application to the simulation of microwave radiances over sandstorms, J. Quant. Spectrosc. Ra., 109, 684–702, 2008.

Huang, J. P., Zhang, W., Zuo, J. Q., Bi, J. R., Shi, J. S., Wang, X., Chang, Z. L., Huang, Z. W., Yang, S., Zhang, B. D., Wang, G. Y., Feng, G. H., Yuan, J. Y., Zhang, L., Zuo, H. C., Wang, S. G., Fu, C. B., and Chou, J. F.: An overview of the semi-arid climate and environment research observatory over the Loess Plateau, Adv. Atmos. Sci., 25(6), 906–921, 2008a.

Huang, J. P., Huang, Z. W., Bi, J. R., Zhang, W., and Zhang, L.: Micro-pulse lidar measurements of aerosol vertical structure over the Loess Plateau, Atmos. Ocean. Sci. Lett., 1(1), 8–11, 2008b.

Huang, J., Fu, Q., Su, J., Tang, Q., Minnis, P., Hu, Y., Yi, Y., and Zhao, Q.: Taklimakan dust aerosol radiative heating derived from CALIPSO observations using the Fu-Liou radiation model with CERES constraints, Atmos. Chem. Phys., 9, 4011–4021, 2009, http://www.atmos-chem-phys.net/9/4011/2009/.

A case study of dust aerosol radiative properties over Lanzhou, China

L. Zhang et al.

Full Screen / Esc

Immler, F. and Schrems, O.: Vertical profiles, optical and microphysical properties of Saharan dust layers determined by a ship-borne lidar, Atmos. Chem. Phys., 3, 1353–1364, 2003, http://www.atmos-chem-phys.net/3/1353/2003/.

Iwasaka, Y., Shi, G. Y., Shen, Z., Kim, Y. S., Trochkine, D., Matsuki, A., Zhang, D., Shibata, T., Nagatani, M., and Nakata, H.: Nature of atmospheric aerosols over the desert areas in the Asian continent: chemical state and number concentration of particles measured at Dunhuang, China, Water Air Soil Poll., 3, 129–145, 2003.

Klett, J. D.: Stable analytical inversion solution for processing lidar returns, Appl. Optics, 2(2), 211–220, 1981.

Klett, J. D.: Lidar inversion with variable backscatter/extinction ratios, Appl. Optics, 24(11), 1638–1643, 1985.

Koren, I., Kaufman, Y. J., Remer, L. A., and Martins, J. V.: Measurement of the effect of Amazon smoke on inhibition of cloud formation, Science, 303(5662), 1342–1345, 2004.

Kovalev, V. A.: Sensitivity of the lidar solution to errors of the aerosol backscatter-to-extinction ratio: Influence of a monotonic change in the aerosol extinction coefficient, Appl. Optics, 34(18), 3457–3462, 1995.

Larchevêque, G., Balin, L., Nessler, R., Quaglia, P., Simeonov, V., Bergh, H. V. D., and Calpini, B.: Development of a mulitwavelength aerosol and water-vapor lidar at the Jungfraujoch Alpine Station (3580 m above sea level) in Switzerland, Appl. Optics, 41(15), 2781–2790, 2002.

Liu, H. Z., Zhang, H. S., Bian, L. G., Chen, J. Y., Zhou, M. Y., Xu, X. D., Li, S. M., and Zhao, Y. J.: Characteristics of micrometeorology in the surface layer in the Tibetan Plateau, Adv. Atmos. Sci., 19(1), 73–88, 2002a.

Liu, Z. Y., Sugimoto, N., and Murayama, T.: Extinction-to-backscatter ratio of Asian dust observed with high-spectral-resolution lidar and Raman lidar, Appl. Optics, 41(15), 2760–2767, 2002b.

McCormick, R. A. and Ludwig, J. H.: Climate modification by atmospheric aerosols, Science, 156(3780), 1358–1359, 1967.

Murayama, T., Sugimoto, N., Uno, I., Kinoshita, K., Aoki, K., Hagiwara, N., Liu, Z. Y., Matsui, I., Sakai, T., Shibata, T., Arao, K., Sohn, B. J., Won, J. G., Yoon, S. C., Li, T., Zhou, J., Hu, H. L., Abo, M., Iokibe, K., Koga, R., and Iwasaka, Y.: Ground-based network observation of Asian dust events of April 1998 in east Asia, J. Geophys. Res., 106(D16), 18345–18359, 2001.

Title Page

Abstract | Introduction

Conclusions | References

Tables | Figures

⏮ | ⏭

◄ | ►

Back | Close

Full Screen / Esc

Printer-friendly Version

Interactive Discussion

Papayannis, A., Balis, D., Amiridis, V., Chourdakis, G., Tsaknakis, G., Zerefos, C., Castanho, A. D. A., Nickovic, S., Kazadzis, S., and Grabowski, J.: Measurements of Saharan dust aerosols over the Eastern Mediterranean using elastic backscatter-Raman lidar, spectrophotometric and satellite observations in the frame of the EARLINET project, Atmos. Chem. Phys., 5, 2065–2079, 2005, http://www.atmos-chem-phys.net/5/2065/2005/.

Pappalardo, G., Amodeo, A., Amoruso, S., Mona, L., Pandolfi, M., and Cuomo, V.: One year of tropospheric lidar measurements of aerosol extinction and backscatter, Ann. Geophys., 46(2), 401–413, 2003.

Pierangelo, C., Chédin, A., Heilliette, S., Jacquinet-Husson, N., and Armante, R.: Dust altitude and infrared optical depth from AIRS, Atmos. Chem. Phys., 4, 1813–1822, 2004, http://www.atmos-chem-phys.net/4/1813/2004/.

Shen, Z. X., Cao, J. J., Li, X. X., Okuda, T., Wang, Y. Q., and Zhang, X. Y.: Mass concentration and mineralogical characteristics of aerosol particles collected at Dunhuang during ACE-Asia, Adv. Atmos. Sci., 23(2), 291–298, 2006.

Su, J., Huang, J., Fu, Q., Minnis, P., Ge, J., and Bi, J.: Estimation of Asian dust aerosol effect on cloud radiation forcing using Fu-Liou radiative model and CERES measurements, Atmos. Chem. Phys., 8, 2763–2771, 2008, http://www.atmos-chem-phys.net/8/2763/2008/.

Twomey, S.: The influence of pollution on the shortwave albedo of clouds, J. Atmos. Sci., 34(7), 1149–1152, 1977.

Wang, S. G., Wang, J. Y., Zhou, Z. J., and Shang, K. Z.: Regional characteristics of three kinds of dust storm events in China, Atmos. Environ., 39, 509–520, 2005.

Xia, J. R.: Lidar measurement of atmospheric aerosol radiative properties over Lanzhou, M. S. thesis, Lanzhou University, China, 50 pp., 2006.

Yamada, M., Iwasaka, Y., Matsuki, A., Trochkine, D., Kim, Y. S., Zhang, D., Nagatani, T., Shi, G. Y., Nagatani, M., Nakata, H., Shen, Z., Chen, B., and Li, G.: Feature of dust particles in the spring free troposphere over Dunhuang in northwestern China: electron microscopic experiments on individual particles collected with a balloon-born impactor, Water Air Soil Poll., 5, 231–250, 2005.

Zhang, L., Chen, M., and Li, L.: Dust aerosol radiative effect and influence on urban atmospheric boundary layer, Atmos. Chem. Phys. Discuss., 7, 15565–15580, 2007, http://www.atmos-chem-phys-discuss.net/7/15565/2007/.

A case study of dust aerosol radiative properties over Lanzhou, China

L. Zhang et al.

Title Page

Abstract | Introduction

Conclusions | References

Tables | Figures

|◄ | ►|

◄ | ►

Back | Close

Full Screen / Esc

Printer-friendly Version

Interactive Discussion

Table 1. Comparison of AOD derived by lidar and sunphotometer
Absolute Difference = $|AOD_{photometer} - AOD_{lidar}|$
Relative Difference = $|AOD_{photometer} - AOD_{lidar}|/AOD_{photometer}$
Ratio Difference = $2(AOD_{photometer} - AOD_{lidar})/(AOD_{photometer} + AOD_{lidar})$.

Case No.	Date_Time (ddmm_hhmm)	$AOD_{photometer}$	AOD_{lidar}	Absolute Diff.	Relative Diff.(%)	Ratio Diff.
1	2603_1209	0.482	0.459	0.023	4.8	0.049
2	2603_1238	0.442	0.449	0.007	1.6	−0.016
3	2603_1307	0.456	0.419	0.037	8.1	0.085
4	2603_1337	0.428	0.381	0.047	11.0	0.116
5	2603_1405	0.419	0.448	0.029	6.9	−0.067
6	2603_1434	0.370	0.448	0.078	21.1	−0.191
7	2603_1503	0.389	0.410	0.021	5.4	−0.053
8	2603_1533	0.449	0.448	0.001	0.2	0.002
9	2703_0830	0.264	0.314	0.050	18.9	−0.173
10	2703_0859	0.265	0.318	0.053	20.0	−0.182
11	2703_0928	0.260	0.263	0.003	1.2	−0.011
12	2703_0957	0.247	0.264	0.017	6.9	−0.067
13	2703_1026	0.253	0.332	0.079	31.2	−0.270
14	2703_1055	0.260	0.311	0.051	19.6	−0.179
15	2703_1124	0.204	0.301	0.097	47.5	−0.384
16	2703_1153	0.235	0.255	0.020	8.5	−0.082
17	2703_1222	0.296	0.303	0.007	2.4	−0.023
18	2703_1251	0.296	0.292	0.004	1.4	0.014
19	2703_1320	0.308	0.333	0.025	8.1	−0.078
20	2703_1349	0.305	0.315	0.010	3.3	−0.032
21	2703_1418	0.271	0.280	0.009	3.3	−0.033
22	2703_1516	0.263	0.298	0.035	13.3	−0.125
23	2703_1545	0.282	0.308	0.026	9.2	−0.088
24	2703_1614	0.296	0.371	0.075	25.3	−0.225
25	2803_1134	1.602	1.565	0.037	2.3	0.023
26	2903_0821	0.446	0.421	0.025	5.6	0.058
27	2903_0850	0.564	0.393	0.171	30.3	0.357
28	2903_0919	0.461	0.417	0.044	9.5	0.100
29	2903_1017	0.394	0.533	0.139	35.3	−0.300
30	2903_1046	0.414	0.448	0.034	8.2	−0.079
31	2903_1115	0.376	0.387	0.011	2.9	−0.029
32	2903_1144	0.412	0.355	0.057	13.8	0.149
33	2903_1213	0.363	0.388	0.025	6.9	−0.067
	Mean			0.041	12.0	−0.055
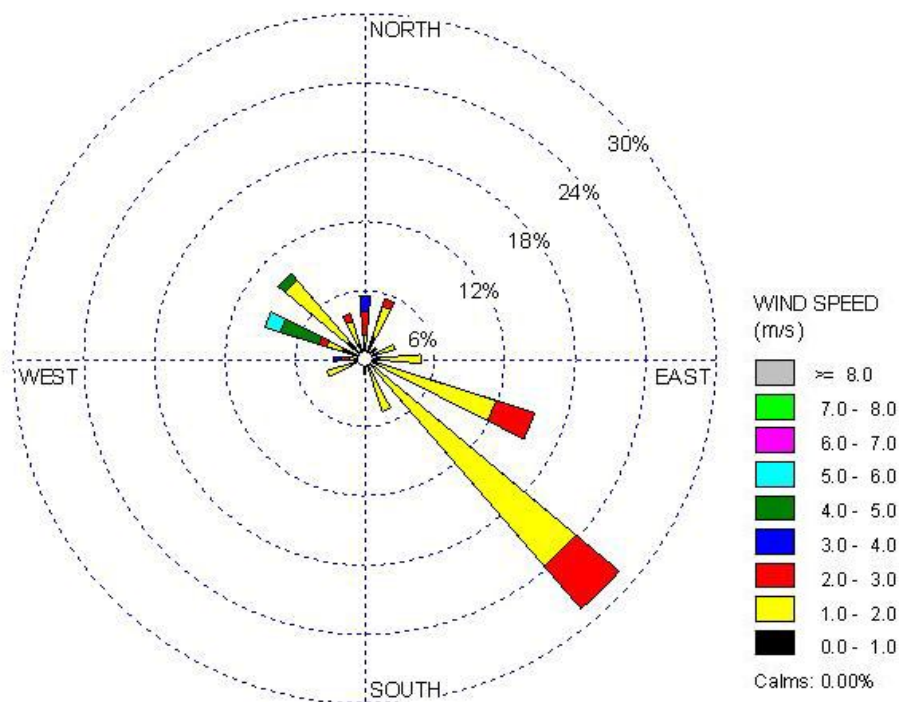
Fig. 1. Wind rose during the dust storm. Wind was observed by a three-axis sonic anemometer 3 m above the ground at SAOCL from 00:00 (Beijing Time) on 27 March to 23:30 on 29 March 2007. Southeast wind was dominant and the speed mainly ranged from 1.0 to 3.0 m/s.
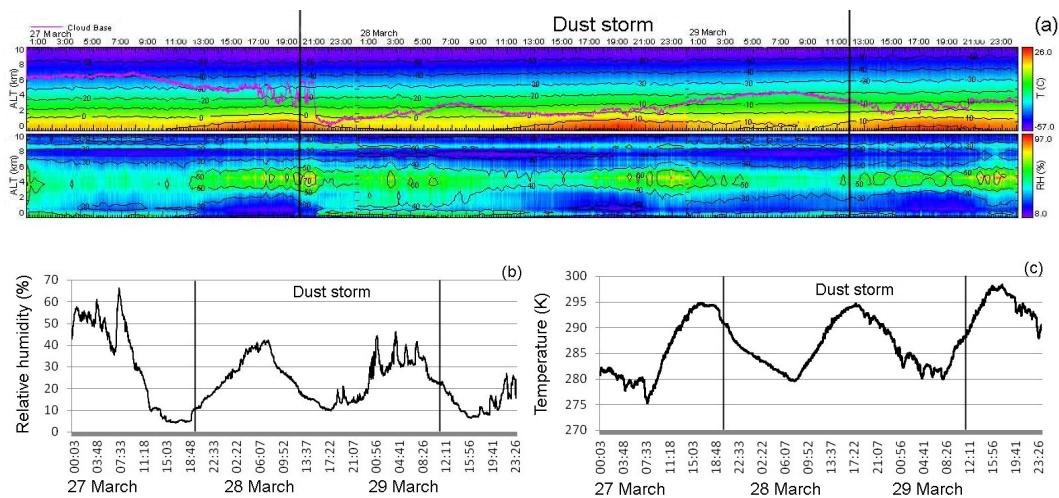
Fig. 2. Temporal evolutions of **(a)** relative humidity and temperature vertical section, **(b)** surface relative humidity, and **(c)** surface temperature. Relative humidity during the dust storm was obviously smaller than that before the dust storm.

2907
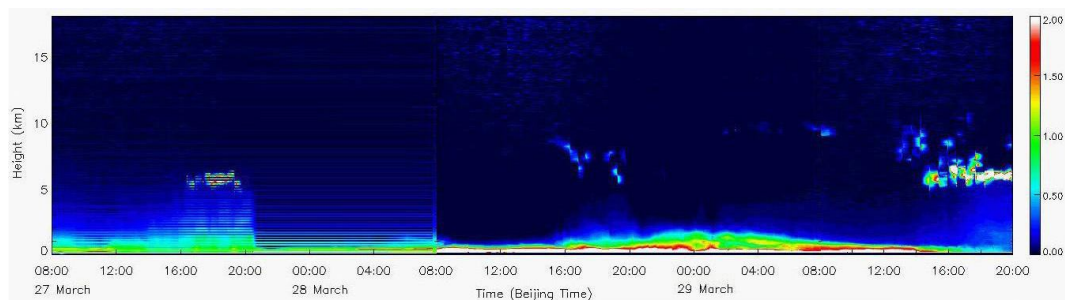
Fig. 3. Temporal evolution of lidar backscattering signal vertical section from 08:00 (Beijing Time) on 27 March to 20:00 on 29 March 2007. It shows that dust aerosol existed mainly below 2 km.
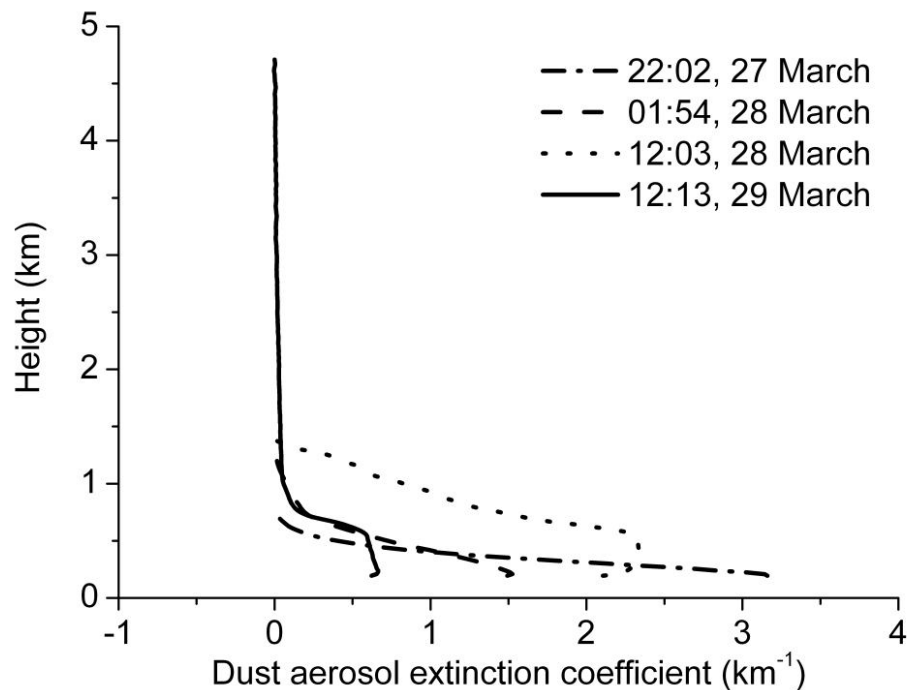
Fig. 4. Vertical profiles of dust aerosol extinction coefficient for four different cases. The dust aerosol extinction coefficient decreased with height.
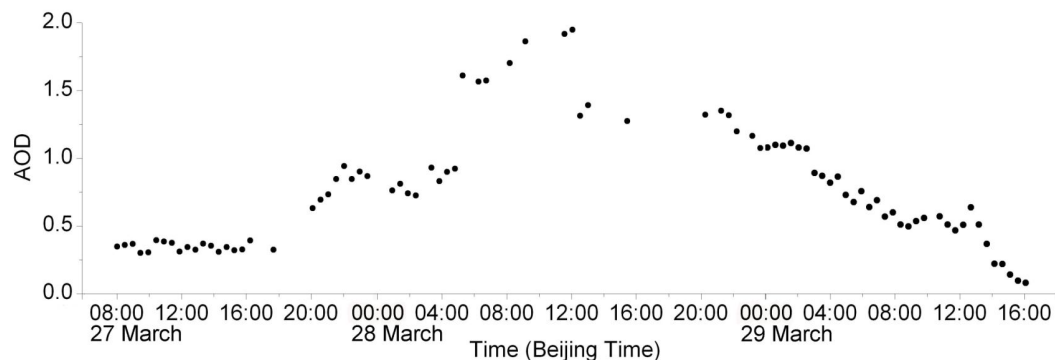
Fig. 5. AOD temporal evolution from 08:00 (Beijing Time) on 27 March to 16:00 on 29 March 2007. The sub-maximum appeared at 22:00 on 27 March and the maximum at 12:00 on 28 March.
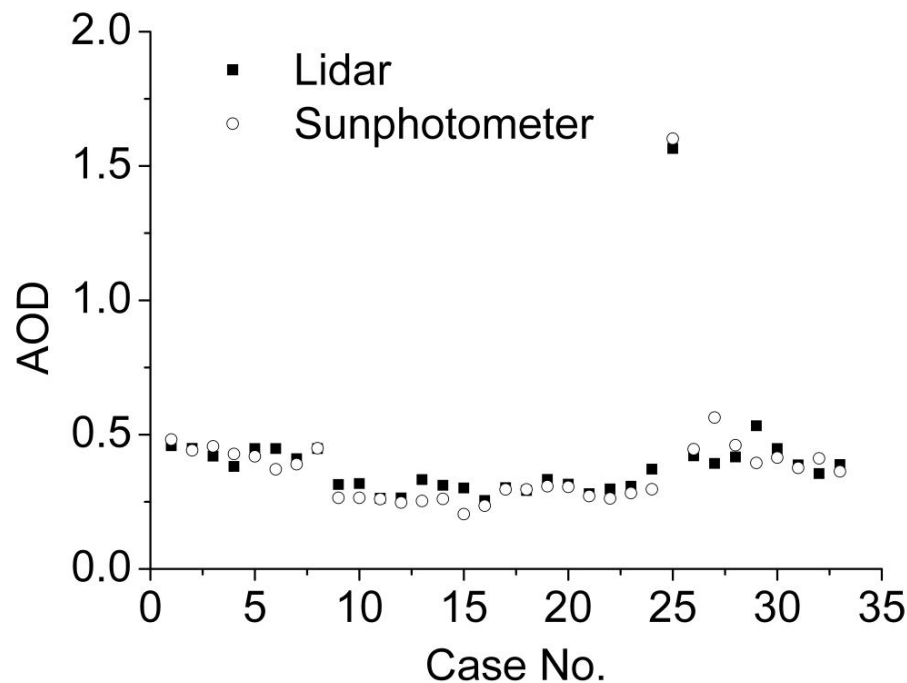
Fig. 6. Comparison of AOD derived by lidar and sunphotometer (Case No. is the same as that in Table 1). It shows a good consistency between two retrievals.
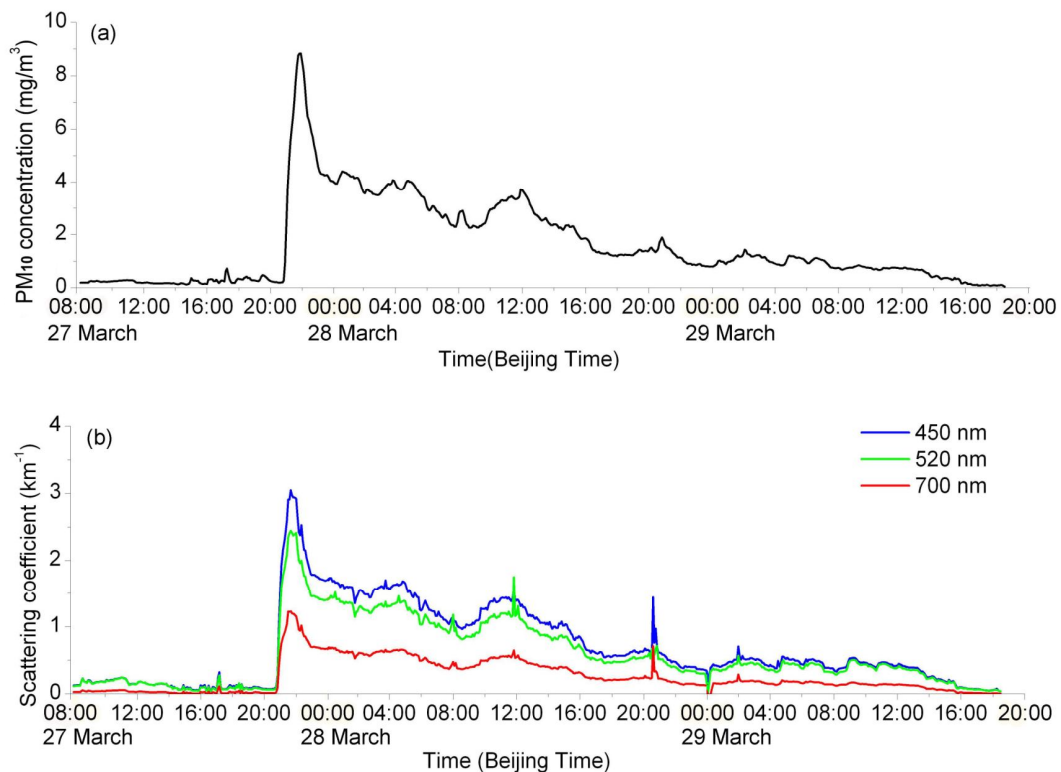
Fig. 7. Temporal evolution of **(a)** PM$_{10}$ concentration and **(b)** aerosol scattering coefficient from 08:00 (Beijing Time) on 27 March to 18:30 on 29 March 2007. The dust aerosol scattering coefficient and PM$_{10}$ concentration had identical variation trends with the maximum at 22:00 on 27 March.

Title Page

Abstract | Introduction

Conclusions | References

Tables | Figures

◀◀ | ▶▶

◀ | ▶

Back | Close

Full Screen / Esc
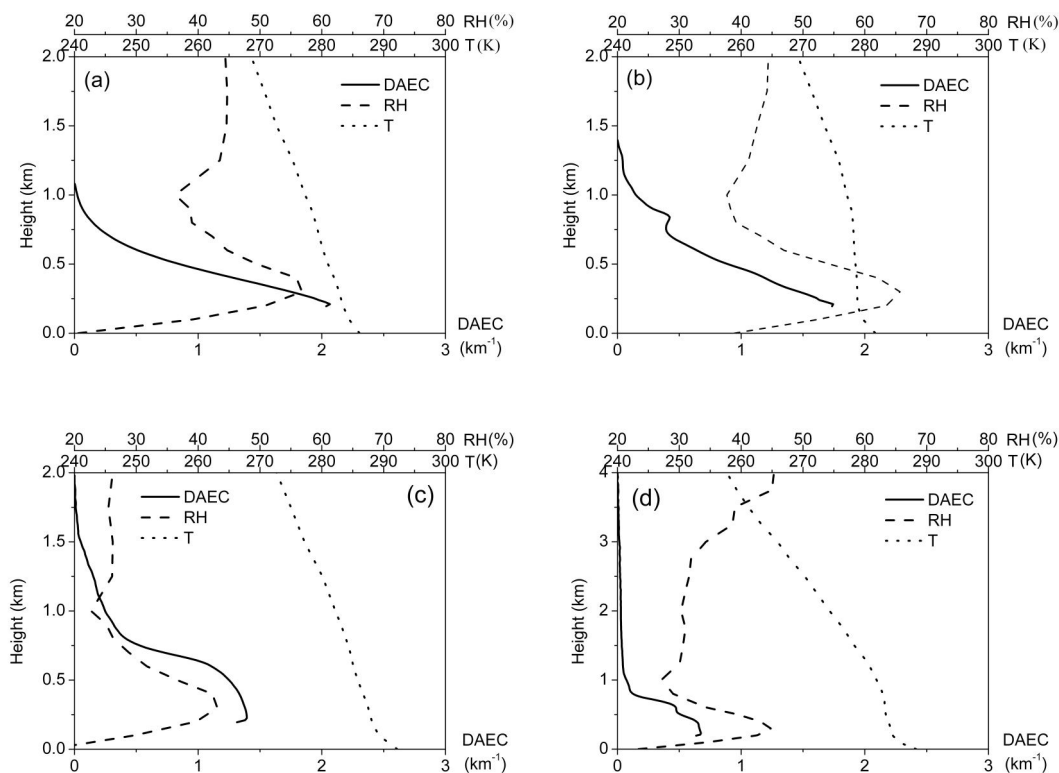
Fig. 8. Vertical profiles of dust aerosol extinction coefficient (DAEC), relative humidity (RH), and temperature (T) at **(a)** 23:00 (Beijing Time) on 27 March, **(b)** 04:48 on 28 March, **(c)** 14:57 on 28 March, and **(d)** 11:15 on 29 March 2007. DAEC and RH showed identical variation trends.
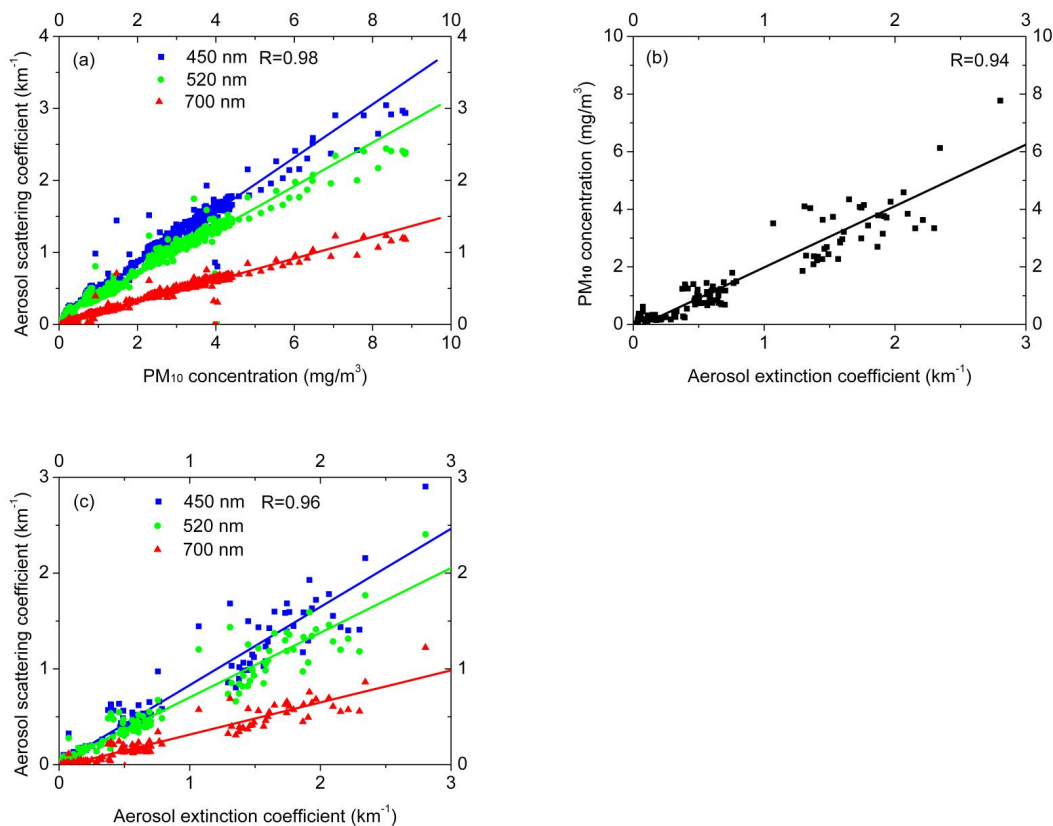
Fig. 9. Correlation among dust aerosol extinction coefficient, scattering coefficient, and PM$_{10}$ concentration.